construction materials

MDPI

Article

Characterization of Ashes from Sewage Sludge–Limestone Incineration: Study of SSA Properties and Reactivity for SCM Use

Danah Shehadeh [1], Alexandre Govin [1,*], Philippe Grosseau [1], Hichem Krour [2], Laetitia Bessette [2], Gonzague Ziegler [3] and Anthony Serclerat [3]

[1] Mines Saint-Etienne, University Lyon, CNRS, UMR 5307 LGF, Centre Spin, F-42023 Saint-Etienne, France; danah.shehadeh@emse.fr (D.S.); grosseau@emse.fr (P.G.)
[2] VICAT, 4 Rue Aristide Bergès, 38080 L'Isle d'Abeau, France; hichem.krour@vicat.fr (H.K.); laetitia.bessette@vicat.fr (L.B.)
[3] FMI Process, 22 Rue de Garat, 42152 L'Horme, France; as@fmi-process.com (A.S.)
* Correspondence: govin@emse.fr

Abstract: This paper examines the properties of sewage sludge ashes (SSAs) from the incineration of sewage sludge with added limestone for toxic gas treatment. It also evaluates the potential valorization of SSA in cement composites as supplementary cementitious materials (SCMs). The work involves a thorough characterization of four SSAs, including physical, chemical, and mineralogical properties. It also includes assessing the behavior of SSA in water solution through electrical conductivity measurements. The reactivity of ashes was evaluated using the R^3 method and mechanical properties. The results revealed that all SSAs present comparable mineralogical and chemical properties, with varying proportions. Major elements such as Ca, Si, Fe, P, and S are predominant in the ashes, with traces of heavy metals. In an aqueous solution, a gradual formation of ettringite was detected only for two SSA. The heavy metal leachability was negligible, confirming that SSA is a non-hazardous waste. Finally, the reactivity and strength activity index assessments revealed a low and slow reactivity of SSA compared to metakaolin or slag. The SSA that favored ettringite formation in aqueous solution presented the lowest compressive strength at 28 days after incorporation in mortar. Despite originating from different incineration sites, these ashes fall under the same category of SCM reactivity.

Keywords: sewage sludge ash; isothermal calorimetry; R^3 test; strength activity index; supplementary cementitious materials

Citation: Shehadeh, D.; Govin, A.; Grosseau, P.; Krour, H.; Bessette, L.; Ziegler, G.; Serclerat, A. Characterization of Ashes from Sewage Sludge–Limestone Incineration: Study of SSA Properties and Reactivity for SCM Use. *Constr. Mater.* **2024**, *4*, 611–628. https://doi.org/10.3390/constrmater4030033

Received: 14 August 2024
Revised: 3 September 2024
Accepted: 6 September 2024
Published: 13 September 2024

1. Introduction

The production of sewage sludge (SS) from wastewater treatment plants is an inevitable by-product of human existence. Sludge management includes mostly agricultural, landfill, and sea disposals. Following the European Union's prohibition on SS sea disposals in 1998, incineration has been developed as an approach for sludge treatment, resulting in a large volume of ash produced [1]. While land application still stands as an option for SS disposal, there are concerns about the potential presence of hazardous elements causing soil contamination. Incineration technology stands as an alternative method for sludge management, providing numerous benefits including a reduction in SS volume by 90%, elimination of organic matter [2], and the added benefit of energy recovery. After incineration, a powdery by-product is generated, commonly known as sewage sludge ash (SSA).

Scientific investigations were applied to determine potential strategies for SSA management. Several studies have been carried out to evaluate its use in cement manufacturing. Some studies considered the use of SSA as an alternative raw material in the kiln during

the production of clinker [3,4]. Other studies investigated SSA usage as supplementary cementitious materials (SCMs), partially replacing cement [5–7]. One common result observed is the porous aspect and irregular morphology of SSA particles, which has led to a higher water demand. As an outcome, a reduction in workability was observed, in addition to an increased porosity of the cementitious composite after SSA incorporation [2,8–10]. Hence, the authors limited the substitution rate to no more than 15% to attain a compressive strength comparable to the reference sample without SSA.

The mechanical properties of the composites with SSA incorporation highly depend on the chemical and mineralogical composition of the ashes. Some ashes were classified as non-reactive (inert) material, limiting their incorporation rate. The authors of [7,11] demonstrated this through a thorough experimental program of testing SSA reactivity through strength activity index (SAI) values and portlandite consumption in SSA/portlandite mixture. Other SSAs, on the other hand, were found to have a hydraulic or a pozzolanic activity, encouraging their use in higher replacement proportions [12]. Pozzolanic SCMs are primarily composed of silicate and aluminate phases that can react with $Ca(OH)_2$ provided by the hydration reaction of cement [13]. The pozzolanic reaction produces calcium silicate hydrates (C-S-H) or calcium aluminate silicate hydrates (C-A-S-H), in addition to the C-S-H formed during the cement hydration [14]. The presence of additional C-S-H improves the mechanical properties of the cementitious composite compared to the reference. Cyr et al. [15] explained that SCMs containing SiO_2 and Al_2O_3 in crystallized form have low reactivity, and, therefore, low pozzolanic activity.

Before considering any application for SSA, it is important to study the environmental behavior in terms of heavy metal content, emphasizing the soluble components rather than the overall metal composition [3]. Świerczek et al. [10] confirm that one additional advantage of incorporating SSA into construction materials is the safe immobilization of harmful heavy metals detected in SSA, hence avoiding environmental risks.

The incineration technology of SS is an example of a cost-effective solution that aligns with circular economy principles. In our study, SSA was collected following SS incineration. Most incineration procedures commonly introduce calcium-based compounds (such as lime or limestone) into the fluidized bed for toxic gas treatment [16]. One specificity of the incineration process used in this work for SSA production is the direct injection of limestone into the SS. Calcium-based additives to the dewatered SS showed good reactivity and efficiency in decreasing sulfur release [17–19]. During carbonization, reactive CaO bonds with sulfur (S) to form $CaSO_4$ [20]. Additionally, in the presence of a high Ca concentration and rich phosphorus (P) fuel mix, Ca-P compounds are observed to form $(Ca_3(PO_4)_2)$ [21,22].

Given this, this study focuses on characterizing the ashes produced by the fluidized bed calcination technique, following the addition of limestone. The data reported in this work offer a comprehensive characterization of four SSA samples, each originating from a different wastewater treatment plant, all employing the same incineration procedure. The paper discusses the ash's physical properties, chemical composition, and mineralogical composition. In addition, SSA behavior in an aqueous solution was determined through the electrical conductivity method. While few studies have investigated the electrical conductivity of SCMs in alkaline or aqueous solutions [23–25], the scope of the investigation has been limited. Our work extends this analysis by measuring the loss in electrical conductivity for 8 days, coupled with multiple sampling over time to assess the behavior of the four ashes in an aqueous solution. Finally, SSA reactivity was examined through chemical and mechanical approaches.

2. Materials and Methods

2.1. Raw Materials

The cement used is an ordinary Portland cement (OPC) CEM I 52.5R CE CP2 NF, with a minimum clinker content of 95%, provided by VICAT. Additionally, four SSAs were used. For this study, four incineration sites were considered. They were located in the

Rhône-Alpes area in France and operated by FMI Process. Sewage sludge (SS), directly received from the wastewater treatment plant, undergoes a drying phase before starting with the incineration process. The incineration technology used on dewatered sludge was the fluidized bed furnace at 850 °C. While incineration primarily evaporates water, organic matter converts into CO, CO_2, NOx, and SOx at 850 °C [26]. To comply with French pollution-control standards, an appropriate amount of limestone ($CaCO_3$) was added to the dewatered SS for effective smoke treatment. After incineration, the produced ashes were collected and stored. The four collected ashes will be named A1, A2, A3, and A4, noting that the SS for A1 production was collected from the biggest site, leading to a higher volume produced per year. The physical properties and oxide composition of the raw materials are summarized in Table 1.

Table 1. Physical properties and oxide composition of OPC and raw SSA.

	OPC	A1	A2	A3	A4
Oxide Content (wt%)					
CaO	62.4	30.8	36.0	47.8	41.8
SiO_2	19.2	20.0	22.0	17.9	16.7
Al_2O_3	4.9	6.4	7.7	3.3	2.5
Fe_2O_3	3.7	15.4	9.1	4.9	8.9
MgO	2.1	1.5	1.5	1.9	1.8
SO_3	3.8	5.3	5.6	4.7	4.8
K_2O	1.0	1.3	1.6	1.6	1.4
Na_2O	0.2	0.4	0.4	0.4	0.3
P_2O_5	0.1	10.3	10.6	10.6	12.7
TiO_2	0.3	0.6	0.6	0.5	0.4
MnO	0.1	0.1	0.1	0.2	0.04
Cl	0.1	0.1	0.1	-	0.2
LOI *	1.6	7.6	4.6	5.8	9.2
Physical properties					
d_{10} (μm)	1.4	1.9	3.4	3.4	2.1
d_{50} (μm)	10.5	23.5	28.1	22.9	19.9
d_{90} (μm)	31.0	109.3	109.6	115.4	92.5
Density (g/cm^3)	3.2	3.0	2.9	2.8	2.7
Specific surface area BET (m^2/g)	1.8	7.8	7.3	5.8	4.6
Moisture content (%)	-	0.4	0.2	0.2	0.20

* LOI: Loss of ignition determined through thermogravimetric analysis at 950 °C.

2.2. SSA Characterization

Particle size distribution was measured using laser diffraction in a dry state using Mastersizer 3000 (Malvern Panalytical) under a pressure of 4 bars and with a vibration rate of 20%. A Helium (He) pycnometer (AccuPyc 1330, Micromeritics) was used to measure real density. In addition, the specific surface area (BET method) was evaluated using ASAP 2020 (Micromeritics). Before analysis, approximately 1 g was degassed for at least 24 h at 100 °C to remove moisture and surface contamination. Following the degassing step, the analysis was performed using the basis of nitrogen gas (N_2) adsorption at −196.2 °C and a relative pressure range (p/p°) from 0.05 to 0.3.

The chemical composition of the ashes was analyzed using X-ray fluorescence (XRF) spectrometry for the determination of the elemental composition expressed as oxide, inductively coupled plasma–mass spectrometry (ICP-MS, Agilent) via the acid attack method (HNO_3 and HCl), and thermogravimetric analysis (TGA) (TG92, Setaram) from 30 to 900 °C with a heating rate of 10 °C/min under He gas flow. Moisture content was measured by determining the mass loss at 105 °C observed with TGA.

The mineralogical content of the four ashes was identified using X-ray diffractometry (XRD) using a Bruker D8-A25 diffractometer equipped with a copper anticathode that emits a wavelength of 1.5406A. The ground powder (less than 100 μm) was backloaded and prepared for analysis. The samples were measured between a 5 and 90° 2θ angle range,

with an increment of 0.02°/s. The mineralogical phases detected were quantified using the Rietveld Refinement, as implemented in TOPAS software (Version 6). The amorphous phase quantification was carried out with the external method using pure corundum as the external standard.

2.3. SSA Behavior in Aqueous Solution

The electrical conductivity of ashes suspension was monitored using a conductimeter, with a water–solid (w/s) weight ratio of 10, over a period of 8 days, until reaching a steady electrical conductivity. This was performed by combining SSA powder with demineralized water in a thermostatic reactor set at 25 °C with constant stirring, which was then sealed with a rubber stopper to avoid carbonation. After obtaining the electrical conductivity curve, SSAs were investigated for their leaching behavior, following a modified European standard, namely, EN 12457-1. The conductivity experiment was repeated, and samples were collected at predetermined time intervals t, selected based on conductivity variations over time. The samples collected underwent a filtration process using a vacuum technique to separate the solid from the liquid. The resulting filtered solid residue, obtained at each time t, was dried at 40 °C for 24 h and then analyzed using XRD. Additionally, the resulting filtered solution or filtrate (9 mL) was diluted with 9 mL of HCl before being analyzed using ICP.

2.4. Reactivity

2.4.1. R^3 (Rapid, Reproducible, Relevant) Test

The R^3 test technique uses a simplified model system that evaluates the pozzolanic activity of SCM individually, avoiding any overlap with the cement hydration reaction. The paste preparation and testing procedure were carried out following RILEM TC 267-TRM. The components used are as followed: m_{SCM} = 11.11 g, $m_{Ca(OH)2}$ = 33.33 g, m_{CaCO3} = 5.56 g, m_{KOH} = 0.24 g, m_{K2SO4} = 1.2 g, m_{water} = 60 g. The solution and the pre-homogenized powders were stored at 40 °C for 24 h [27]. The paste was prepared by mixing the powder with the solution for 60 s. After mixing, a mass of approximately 9 g was placed in a plastic cell and was introduced into the channel of an isothermal TAM-Air calorimeter regulated at 40 °C. The calorimeter records the heat released during the testing period. After testing, the heat flow and cumulative heat flow were calculated for up to 7 days and were normalized with respect to SSA mass.

After 7 days, the samples were removed, ground to less than 100 µm, and the ongoing hydration reaction was stopped, using the solvent (isopropanol) exchange method [28]. This technique replaces water in pores with isopropanol to block any hydration reaction. The ground particles were rinsed with isopropanol solution twice and then immersed with diethyl ether. The samples were then vacuumed and dried in the oven at 40 °C for 24 h. Consequently, the dried samples were analyzed using TGA for bounded water (at 350 °C) and portlandite content (between 350 °C and 450 °C). Portlandite consumption was calculated following Equation (1). A correction was made to account for the initial portlandite content in raw ashes.

$$\%Ca(OH)_{2\ consumed} = (\%Ca(OH)_{2\ initial} + \%Ca(OH)_{2\ SSA}) - \%Ca(OH)_{2\ remaining} \quad (1)$$

where

$Ca(OH)_{2\ initial}$: Total mass of portlandite introduced for R^3 test
$Ca(OH)_{2\ SSA}$: Total content of portlandite and calcium oxide in raw SSA determined initially by XRD
$Ca(OH)_{2\ remaining}$: Total content of portlandite after 7 days of R^3 test determined by TGA

2.4.2. Strength Activity Index (SAI)

The mechanical properties of the SSA-blended cement mortars were examined. Mortars were manufactured according to French Standard NF EN 450-1, with SSA replacing

25 wt% of OPC. The masses of mortar components are as follows: $m_{cement+SSA}$ = 450 g, m_{sand} = 1350 g, with a water-to-binder ratio of 0.5. After mixing, the samples were placed in 4 × 4 × 16 cm^3 molds, de-molded after 24 h, and stored in a chamber at 20 °C and humidity higher than 95%, until the testing period. The compressive strength was evaluated at 1, 2, 7, and 28 days. SAI was calculated using Equation (2).

$$SAI(\%) = \frac{Rc_i}{Rc_{reference}} \times 100 \quad (2)$$

where

Rc_i: Compressive strength of the SSA-modified mortar at time t
$Rc_{reference}$: Compressive strength of the reference mortar without SSA at time t

3. Results

3.1. Properties of SSA

The physical, chemical, and mineralogical properties of SSA were evaluated, providing a better understanding of SSA behavior and environmental impact.

3.1.1. Physical Properties

In general, the physical properties of the ashes are highly influenced by the incineration process, the post-incineration treatment, and the storage conditions. Table 1 presents the studied physical properties of the cement (OPC) and the four ashes (A1, A2, A3, and A4). The particle size distribution of OPC and SSA is measured and represented by d_{10}, d_{50}, and d_{90} in Table 1. The results indicate variations between the cement and the ashes. The particle size distribution of the ashes extends between 0.1 µm and 200–500 µm with a d_{50} ranging between 20 µm and 28 µm, greater than that of OPC with a value of 10.5 µm. OPC has the lowest d_{10}, indicating finer particles. While the d_{90} for OPC is 31 µm, the d_{90} for SSA ranges from 92.5 µm (A4) to 115.4 µm (A3). This indicates that all SSA hold larger particles than the cement. It also indicates that A3 has the biggest proportion of large particles compared to other SSA. The density values of the four SSAs and the cement, ranging from 2.7 to 3 g/cm^3 and 3.2 g/cm^3, respectively, showed a slightly lower density than that of cement. As for the specific surface area of SSA, the values ranged from 4.6 m^2/g for A4 to 7.8 m^2/g for A1. These values are significantly higher than that of OPC (1.8 m^2/g). This was confirmed by Cyr et al. [15]. These findings suggest a porous nature for SSA particles, which may lead to an additional demand for water [29]. The ashes present a negligible moisture content of less than 0.35%, attributed to the high incineration temperature of 850 °C.

3.1.2. Chemical Properties

The chemical composition of the ashes, obtained using XRF in the form of oxide, is detailed in Table 1. The ashes mainly contain calcium (Ca), silica (Si), phosphorus (P), iron (Fe), and aluminum (Al). The content of Si and Al in the form of oxide ranges from a minimum of 17% and 2.5% for A4 and a maximum of 22% and 7.7% for A2, respectively. This may contribute to the pozzolanic reaction of the ashes and consequently enhance their reactivity if available in the amorphous phase [30].

The collected ICP results for the four SSAs, presented in Table 2, confirm the predominance of Ca as a main element. Additionally, the content for P, Fe, S, and Al was consistent with the elemental composition determined using XRF analysis. Unlike in XRF, the Si element was not detected since sample preparation was performed using the acid attack method, as it has poor efficiency for Si elements. The ICP findings align with XRF data, revealing Ca as the main element, raised Fe levels, particularly in A1, and a notable P content.

Table 2. Chemical composition of raw SSAs using ICP (in mg/kg dry mass).

	Concentration (mg/kg Dry Mass)	A1	A2	A3	A4
Major Elements	Ca	200,080	178,440	273,160	265,390
	Fe	120,070	68,710	33,580	61,330
	P	45,620	41,780	43,350	52,800
	Al	32,840	49,670	15,560	8960
	S	24,140	29,080	21,600	23,460
	K	13,170	15,400	15,290	11,600
	Na	2860	4930	270	2640
Minor Elements	Mn	1762	1171	1026	239
	Zn	1178	992	1189	1262
	Cu	509	473	920	902
	Cr	227	159	68	80
	Se	134	234	209	134
	Pb	133	98	31	92
	Ni	nd	nd	45	745
	Mo	19	18	12	12
	Co	nd	nd	9	7
	As	7	5	12	7
	Cd	2	3	1	2
	Ba	0.6	0.7	0.3	0.6

Furthermore, the ICP data show trace amounts of heavy metals, with Mn, Zn, Cu, Cr, Se, and Pb being the most predominant. After SS incineration, a significant reduction in volume is observed, leading to a higher concentration of heavy metals in SSA [10]. Based on the results in Table 2, variations in heavy metal concentration were observed among the four different SSAs.

The thermal analysis carried out on the four SSAs is presented in Figure 1a. The results allow the identification of three main peaks: one dehydration peak between 50 and 105 °C, and two thermal decomposition peaks assigned to portlandite ($Ca(OH)_2$) between 350 and 450 °C and to calcite ($CaCO_3$) between 515 and 750 °C. The quantification results in Figure 1b show $Ca(OH)_2$ content of 1% for A2, 3.3% for A1 and A3, and a significantly higher value of 7.1% for A4. Additionally, $CaCO_3$ content is about 10% in all SSA, except for A4, which shows a higher value of 16.5%. It is worth noting that a common step for the four incineration processes is the addition of limestone into SS to reduce toxic gas emissions, which is the main reason for the high $CaCO_3$ content. The increase in $CaCO_3$ content for A4 may be attributed to an excess of limestone added during this specific incineration batch. In addition, inadequate storage conditions may cause the material to be exposed to air (humidity and CO_2) and result in the hydration and carbonation of CaO in the ashes, leading to additional $Ca(OH)_2$ and $CaCO_3$, respectively.

3.1.3. Mineralogical Composition

The XRD qualitative analysis is illustrated in Figure 2 and reveals that the studied ashes are multiphasic materials. After incineration, the ashes have no organic matter but some crystallized minerals [30]. The quantitative analysis of the crystallized phases is presented in Table 3. Based on the results obtained, all four SSAs have common major crystallized mineral phases such as whitlockite ($Ca_9Mg_{0.7}Fe_{0.5}(PO_4)_6(PO_3OH)$), illite ($K_{0.6}(H_3O)_{0.4}Al_{1.3}Mg_{0.3}Fe_{0.1}Si_{3.5}O_{10}(OH)_2{\cdot}(H_2O)$), calcite ($CaCO_3$), quartz ($SiO_2$), biotite ($KMg_{2.5}Fe_{0.5}AlSi_3O_{10}(OH)_{1.75}F_{0.25}$), and albite ($NaAlSi_3O_8$), as well as soluble phases such as lime (CaO), anhydrite ($CaSO_4$), and portlandite ($Ca(OH)_2$). Ca is mainly present in whitlockite, lime, anhydrite, and calcite, which explains its dominance in XRF and ICP. The presence of anhydrite, a source of sulfate, is consistent with the presence of sulfur in oxide form (see Table 1). During incineration, the limestone transforms into calcium oxide (CaO) through calcination, which, in turn, reacts with sulfur gases (SO_2) to form

calcium sulfate or anhydrite [31]. Phosphorus is known to disturb the hydration reaction of cement by delaying its setting time [32]. However, according to XRD results in Figure 2, P is found to be in whitlockite, which is known to be a weakly soluble phase in an alkaline solution. The crystallized silicon oxides (quartz and cristobalite) available in SSA could be a sand residue from the fluidized bed or natural sources (such as minerals found on the Earth's surface) [33]. The presence of Fe_2O_3 is responsible for the reddish color of the ashes, particularly observed for A1, which presents the highest percentage (7%). Haustein et al. [5] observed the same distinctive dark red coloration with a 12% Fe_2O_3 content in their ashes.

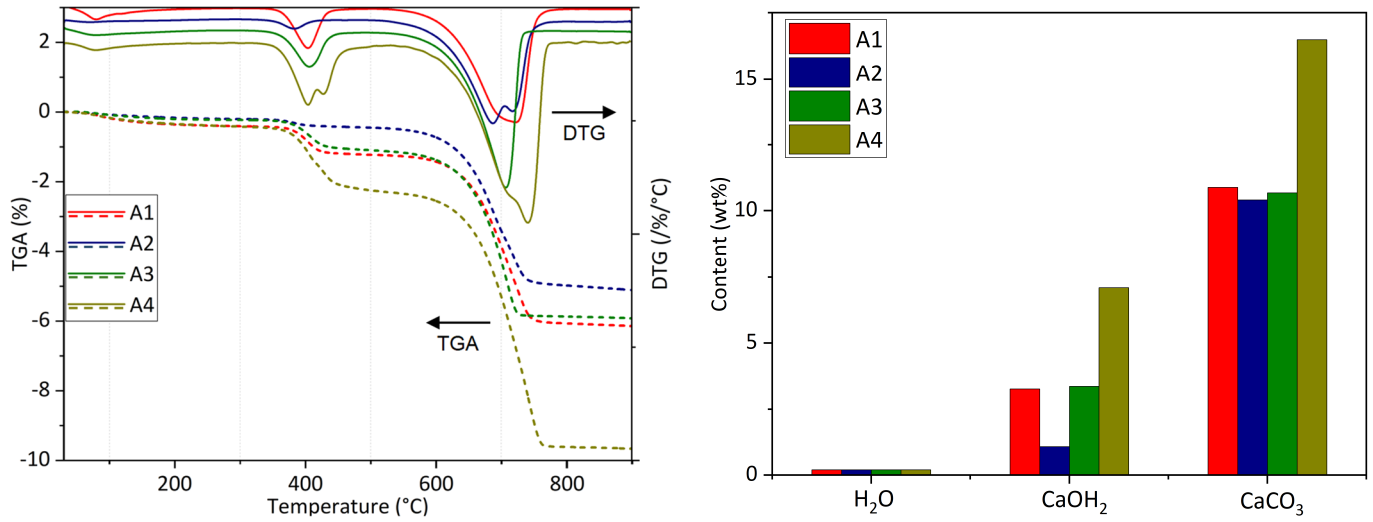

Figure 1. Thermal characterization: (**a**) curves of ATG in dashed lines, DTG in solid lines, and (**b**) TG quantification of raw SSA.

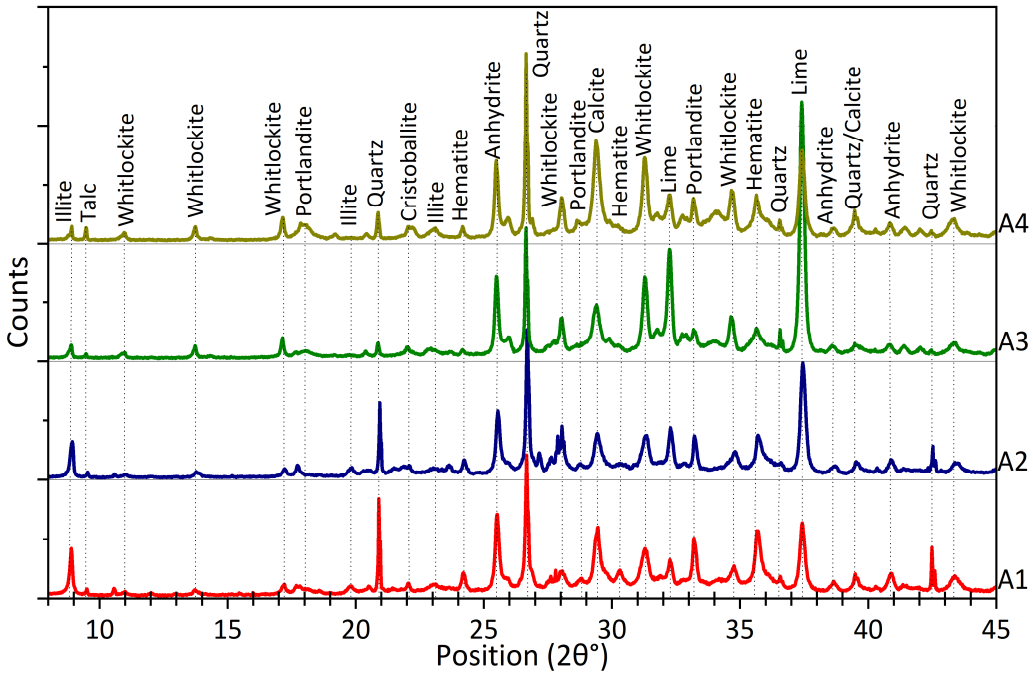

Figure 2. XRD signal of the four SSAs.

Table 3. Mineralogical content of raw SSA in wt%.

Mineralogical Phases (wt%)	A1	A2	A3	A4
Whitlockite	11	10	15	19
Calcite	9	8	10	17
Illite	9	10	2	6
Hematite	7	5	4	4
Anhydrite	7	5	7	6
Lime	6	10	20	6
Quartz	5	9	5	6
Biotite	5	4	1	-
Portlandite	4	1	4	7
Dolomite	2	2	5	5
Albite	3	2	1	1
Other	5	7	6	3
Amorphous	28	28	20	18

According to Donatello et al. [3], who provided an overview of incinerated SSA, common crystalline phases such as quartz, whitlockite, and hematite are frequently identified. $CaCO_3$ and $Ca(OH)_2$ values were consistent with the TGA results. Juenger et al. [29] investigated new sources of reactive SCM and stated that high content in the amorphous phase favorizes the material's reactivity. The quantified amorphous phase of SSA, according to Table 3, ranged from 18% for A4 to 28% for A1 and A2. This statement helps to classify the studied SSA as a potential SCM source. The amorphous phase is the active component of a pozzolanic SCM. Moreover, amorphous Si and Al serve as an indicator of the reactivity potential of the ashes [30].

Using the data collected from XRF, ICP, and XRD, we employed an analytical approach to determine the mass percentage of each chemical element present in SSA using Equation (3). This method was applied to XRD data. The XRF data, originally expressed in oxide form as shown in Table 1, are recalculated into elemental percentages. After calculation, a comparative analysis was performed using the percentages of each element obtained from each characterization method. If the results from ICP and XRF were higher than those of XRD, then it indicates that the calculated element is by default present as an amorphous phase in the ashes. The findings suggest that the amorphous phase mostly consists of Ca as a major element, with Fe, Si, and P present as minor elements. This observation was consistent among the four examined SSAs. This implies that Si and Al are mainly present in crystallized rather than amorphous form. As a result, the pozzolanic activity of the studied SSA is expected to be low [14].

$$W_i = \sum_j \left[\left(\frac{W_j}{Mj} \right) \cdot M_i \right] \quad (3)$$

where

W_i: Weight percentage of each chemical element i to be determined in wt%
W_j: Weight percentage of each phase j determined by XRD in wt%
M_j: Molar mass of phase j in g/mol
M_i: Molar mass of element i in g/mol

3.2. Electrical Conductivity in Water Solution

The electrical conductivity curves in Figure 3 show a similar global tendency for the four SSAs after contact with water. The rapid increase in electrical conductivity is governed by the rise in ion concentration in the solution from the dissolution of soluble species [34]. The increase in electrical conductivity for the ashes in Figure 3 reached a value of 13.3 mS/cm for A2 and A3 and 12.3 mS/cm for A1 and A4, after 1 min of immersion. This increase is followed by a drop in electrical conductivity, indicating a precipitation

phenomenon. After 2 h, A1 and A2 exhibited a faster decrease of 2.5 mS/cm over the 8 days. This suggests that A1 and A2 may experience an accelerated precipitation compared to the other two SSA, which showed a slower decrease in conductivity of 1.5 mS/cm. Based on the XRD quantification results in Table 3, A2 and A3 present the highest content of water-soluble phases (mainly CaO and $CaSO_4$) and are expected to show the highest electrical conductivity upon contact with water. The test results show a notable similarity in the behavior of the four ashes. The maximum dissolution happens immediately after contact with water, and no further dissolution or significant precipitation occurs after 50 h (almost 2 days). As shown in Figure 3, the high increase in conductivity is spotted along with an immediate increase in pH after contact with water. A pH level higher than 12 was attained for the four SSAs and remained constant during the testing. The high pH level indicates a highly alkaline medium. This suggests that the results obtained from this test would most likely be comparable if a $Ca(OH)_2$ solution was used instead of deionized water. Based on these observations, it is reasonable to expect the ashes to behave similarly after incorporation into cementitious composites. This is supported by the fact that the pH in the bulk solution rises during cement hydration, with $Ca(OH)_2$ being one of the primary formed hydrates [35,36]. Additionally, the presence of SSA in cement composites may increase the $Ca(OH)_2$ formed, which modifies the microstructure of the composite, affecting its durability properties.

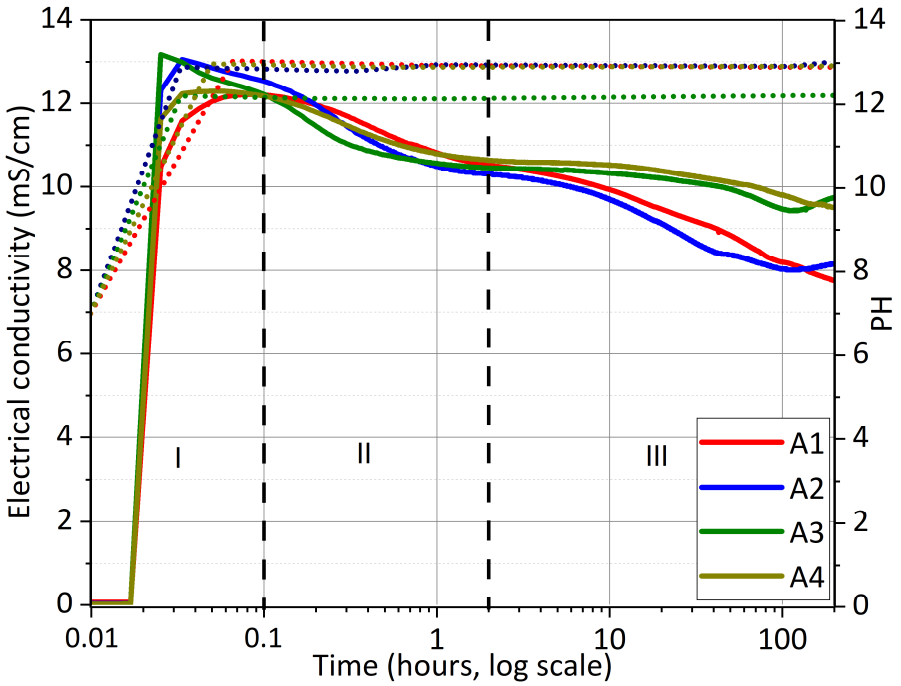

Figure 3. Conductimetry of the ashes in an aqueous solution with pH tracking illustrated in a dotted line.

De Azevedo Basto et al. [24], linked the electrical conductivity variation to the pozzolanic activity of SCM. They concluded that the constant conductivity over time indicates the absence of a pozzolanic reaction. Additionally, Delair et al. [25] stated that the decrease in conductivity is influenced by the pozzolanic activity of the tested material. Paya et al. [23] clarified that the early-stage reactions are primarily governed by the dissolution phenomena. They added that the reactive amorphous content remains unreacted initially but tends to undergo a slow reaction over the long-term stages. According to the findings in Figure 3, the conductivity of the SSA–water mixture is slowly decreasing over 8 days, suggesting a potential for low pozzolanic activity. In line with the analysis of Delair et al. [25], A1 and A2 are classified as having a pozzolanic reactivity moderately higher than that of A3 and A4.

3.3. Sampling over Time

To better understand the mineralogical and the chemical evolution of the four ashes after contact with water, and to analyze the heavy metals leached over time, samples were collected at different time intervals, for each SSA. This was carried out according to a modified European standard, namely, EN 12457-1. As illustrated in Figure 3, the electrical conductivity of the four solutions was split into three stages. Stage I, up to 0.1 h (6 min), reflects the immediate reactions upon immersion. Stage II, between 0.1 h and 2 h, where a rapid drop in electrical conductivity occurs for the four ashes similarly. Stage III, extending up to 200 h (8 days), where a slight divergence was observed for A1 and A2 on one side and A3 and A4 on the other side. The samples were collected according to the curve variations and are as follows: one sample from stage I (I1), two samples from stage II (II1 and II2), and one sample from stage III (III1).

3.3.1. Mineralogical Analysis of Filtered Solid

Figure 4 (on the left side) presents the XRD signals of filtered solid samples at stages I1, II1, II2, and III1.

One common behavior detected for all samples is the immediate dissolution and hydration of CaO within a few minutes upon immersion, highlighted by the disappearance of the main peak at 2θ = 37.5° and the appearance in the pic at 2θ = 18° assigned to $Ca(OH)_2$. A3, having the highest content in CaO (20%) presents the highest peak intensity of portlandite or $Ca(OH)_2$ (Figure 4c), confirming the instant transformation of CaO into $Ca(OH)_2$. Lime is known to be extremely reactive and has a high dissolution rate in water, resulting in a quick pH increase (and sometimes temperature increase), as shown in Figure 3. The constant stirring also helps increase its dissolving rate. No other crystallized phase disappeared besides CaO at I1, implying that the increase in electrical conductivity in Stage I is mainly governed by CaO dissolution. $CaSO_4$ peak at 2θ = 25.2° shows a proportional decrease in intensity with time until total disappearance in III1. This was commonly observed for the four ashes and is linked to the dissolution rate of this compound in these experimental conditions. Besides the precipitation of $Ca(OH)_2$ with an intense peak at 2θ = 18°, ettringite ($Ca_6Al_2(SO_4)_3(OH)_{12}{\cdot}26H_2O$) was detected only in Figure 4c,d. Even though the same w/s ratio was used for all four solutions, only A3 and A4 showed ettringite formation, with a small peak observed in Stage II, and a more defined peak for III1. Elements released into the solution are controlled by SSA chemical composition; therefore, the formation of secondary phases is mainly driven by different stoichiometric ratios of elements in the solution [37]. It is also highly probable that secondary phases might have been formed as poorly crystallized or amorphous phases and were not detected using XRD analysis. The slight increase in $CaCO_3$ peak intensity (Figure 4a) could be due to the carbonation of the collected samples after exposure to air and humidity.

3.3.2. Chemical Analysis of Filtrate

The filtrate analysis is illustrated in Figure 4 (on the right side), showing the concentration evolution of the major elements leached, in parallel to the electrical conductivity curve. Heavy metals are detailed separately in a table and compared to the European standard limits [38]. According to the graphs in Figure 4, similar tendencies in concentration evolution are observed across all four ashes. Ca and S are the common abundant elements in all the collected samples, with a concentration higher than 0.1 mol/L over time. Ca concentration decreases slightly from Stage I to Stage II, followed by a more pronounced decrease in Stage III, particularly for A1 and A2. On the other hand, S concentration increases from Stage I to Stage II, followed by a decrease in Stage III, commonly observed for the four ashes. The increase in Ca ion concentration in Stage I is due to the total dissolution of CaO, as detailed in Section 3.3.1, and the drop in Stage II and Stage III is partially a consequence of $Ca(OH)_2$ precipitation for all ashes. The increase in S ion concentration spotted in both Stages I and II is attributed to the gradual dissolution of $CaSO_4$, as discussed in the previous section. In the case of A3 and A4, the drop of both Ca and S ion concentrations in Stage III results

from ettringite precipitation. The reduction in Ca ions in Stage III may also be linked to the formation of amorphous C-S-H or C-A-S-H, which are weakly crystallized products from the pozzolanic reaction [39]. We expect a slightly higher precipitation of hydrates in the case A1 and A2. This is confirmed by the significant reduction in Ca concentration for A1 and A2 in Stage III, which is linked to a greater formation of hydrates. This correlation aligns with the electrical conductivity analogy in 3.2 and supports the conclusion regarding the slightly improved pozzolanic activity of A1 and A2.

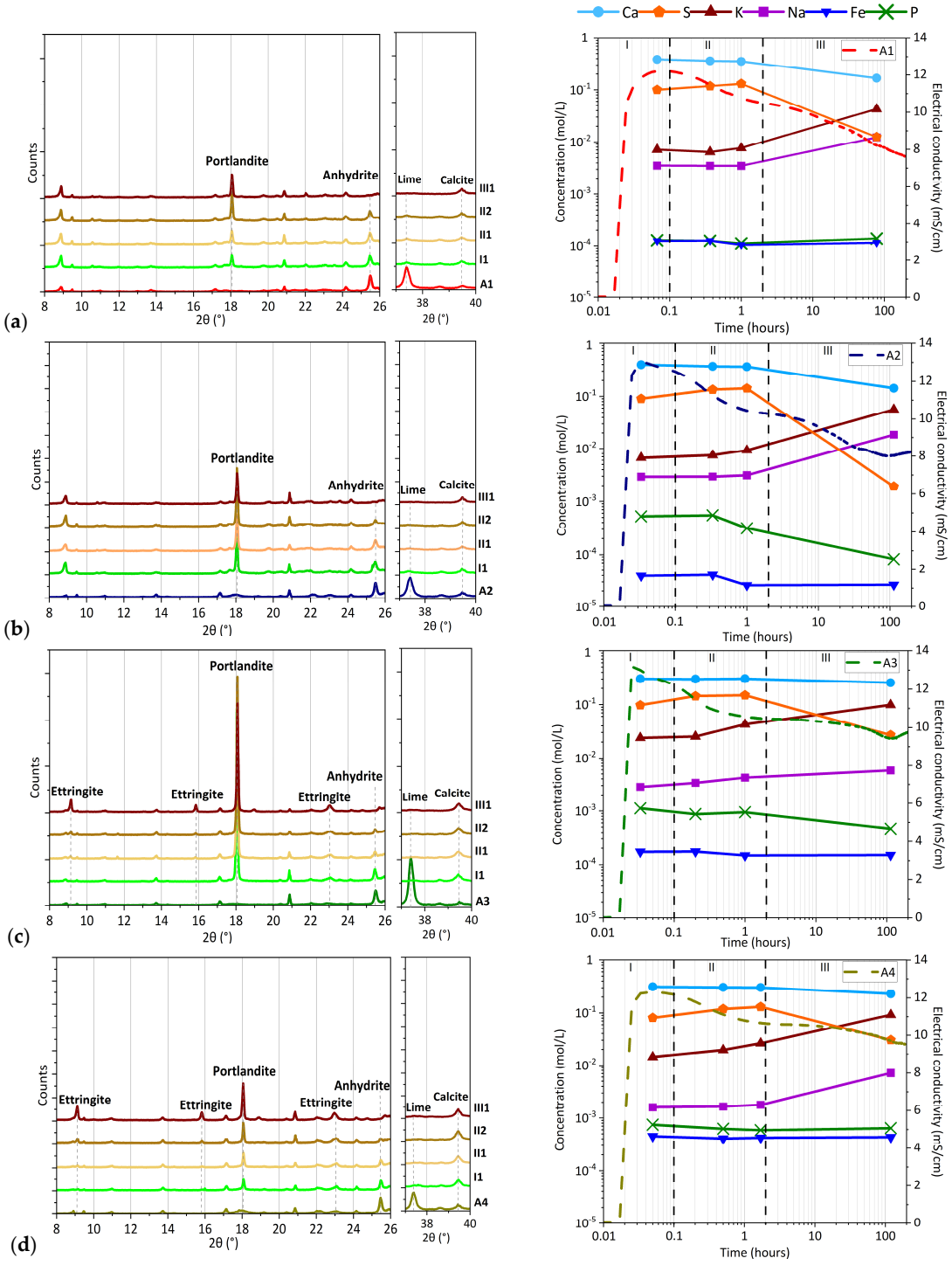

Figure 4. XRD of filtered solid, on the left side, and ICP analysis of filtrate (mol/L), on the right side, for (**a**) A1, (**b**) A2, (**c**) A3, and (**d**) A4.

Minor elements, such as K and Na, showed a slight rise in concentration over time, reaching around 0.1 mol/L in Stage III for A3 and A4 in the case of K and below 0.05 mol/L for Na. These elements are found in mineral crystalline phases (illite, biotite, and albite) and the amorphous phase in negligible quantities. Fe and P elements exhibit low concentrations. No significant variations in concentrations were detected, indicating their limited presence in the solution. This confirms the low solubility of mineral phases containing these elements in basic media, such as whitlockite, hematite, and talc.

As for the concentration of heavy metals presented in Table 4, the results are quite different for the four ashes, reflecting the variability in concentration within the raw sewage sludge. All the data revealed a leachability concentration lower than the limits imposed by the French regulations [40], implying that the studied SSA is classified as non-hazardous waste. Zn presents a concentration higher than the inert limit value except for A2, having initially a lower concentration with respect to other ashes. The Pb and Ba concentrations in A3 and A2, respectively, are higher than the inert limit. According to Chang et al. [41], heavy metals may be absorbed into the structure of cement hydration products. Then, SSA incorporation in cement composites reduces the heavy metal leaching problem.

Table 4. The concentration of leached heavy metals at point III1.

Leached Elements	Concentration (mg/kg Dry Mass)				Limit * (mg/kg Dry Mass)	
	A1	A2	A3	A4	Inert	Non-Hazardous
Cr	1.0	0.1	3.5	0.0	0.5	10
Ni	0.0	0.0	0.0	0.0	0.4	10
Cu	0.2	0.0	0.5	0.9	2	50
Zn	27.5	3.4	4.6	10.3	4	50
Mo	2.3	0.6	2.5	2.1	0.5	10
Cd	0.0	0.0	0.0	0.0	0.04	1
Pb	0.3	0.2	0.6	0.0	0.5	10
As	0.0	0.0	0.0	0.0	0.5	2
Ba	8.9	74.4	15.3	0.1	20	100
Se	0.0	0.0	0.1	0.0	0.1	0.5

* Limit: Refers to the concentration of leached element used to categorize the type of waste, as specified in the French regulations [40].

3.4. Reactivity of SSA

While projecting the use of SSA as SCM in cementitious composites, the study of the reactivity is important. This step helps determine the presence of a pozzolanic activity, which generates additional hydrates and improves the mechanical properties of the final composite. One technique to assess reactivity involves monitoring the heat released during the first 7 days of hydration, at 40 °C, using isothermal calorimetry [42]. In addition, Ali et al. [43] adopted the use of bounded water and portlandite consumption values as a rapid technique to predict the long-term reactivity of SCM.

3.4.1. Reactivity Assessed Using the R^3 Method

The heat release of the four mixtures was recorded and presented in Figure 5a. During the first hour, all four ashes showed an increase in the heat release, indicating the dissolution phenomena in the solution. This corresponds to Stages I and II of Figure 3, governed primarily by the dissolution of CaO and $CaSO_4$ content in SSA. Afterwards, a brutal decrease in the heat signal is noticed and a minor peak for A1 and A2 was detected at around 5 and 12 h, respectively. The signal was then observed to be low and stable over the testing period. The cumulative heat flow shows a gradual increase over time, indicating that the ongoing reaction is slow. The calculated cumulative heat at 7 days gives a value of 180 J/g and 162 J/g SSA for A2 and A1, and a lower value of 107 J/g and 80 J/g SSA for A3 and A4, respectively.

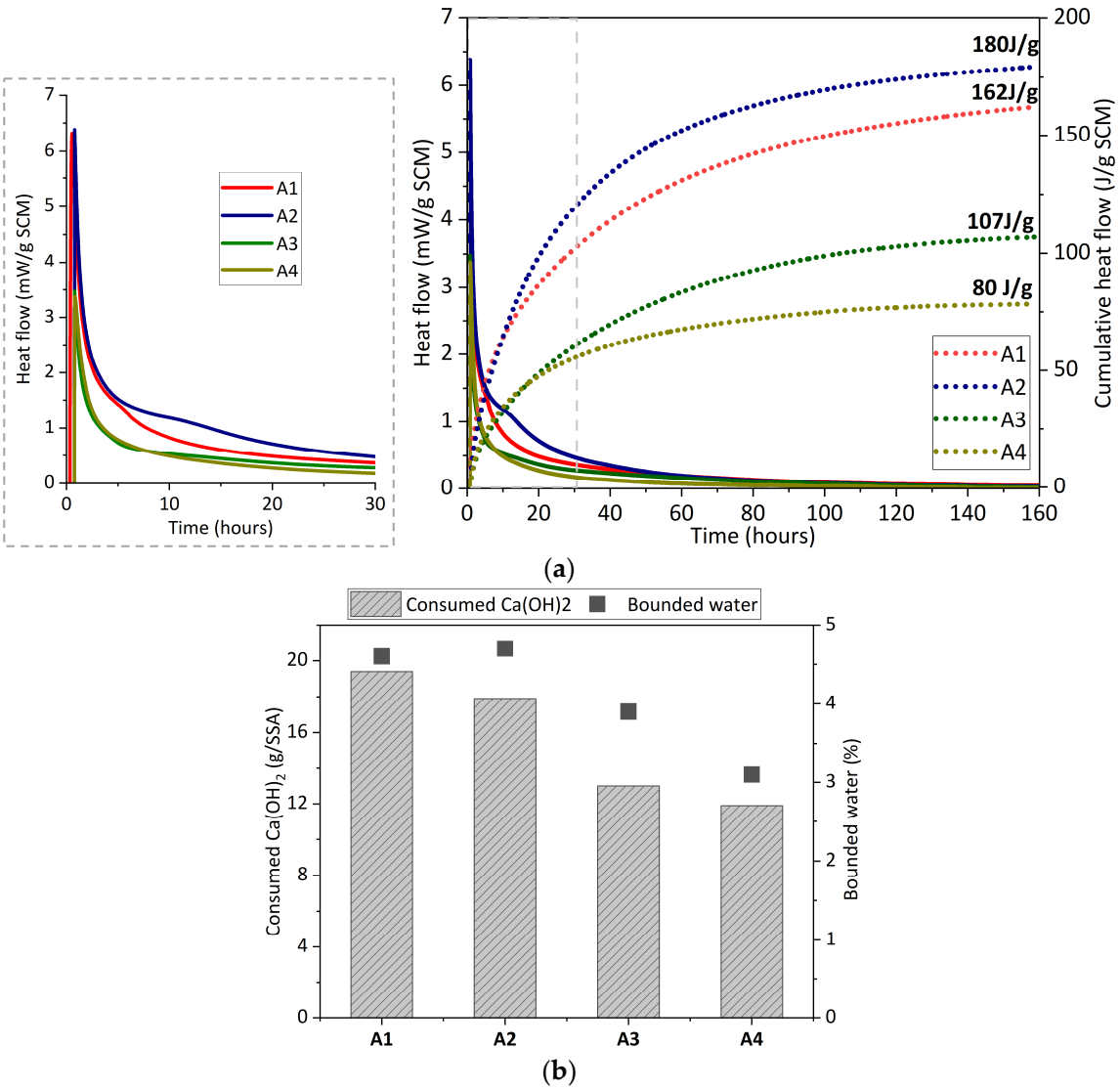

Figure 5. SSA reactivity evaluated using the R^3 method (**a**) calorimetry analysis and (**b**) hydroxide consumption and bounded water.

Figure 5b summarizes the bounded water content and the consumed portlandite percentage at 7 days. The bounded water percentage was determined using TGA, up to 350 °C. Avet et al. [42] stated that bounded water is a direct indicator of the material's reactivity as it corresponds to the decomposition of the main hydrates. A2, with the highest bounded water content of 4.7%, presents a slightly higher reactivity than A4, which has the lowest value of 3.1%. This observation aligns with the cumulative heat results previously presented. A1 and A2 present a $Ca(OH)_2$ consumption of 19.4 g/g SSA and 18 g/g SSA, respectively. A3 and A4, on the other hand, exhibit a reduced $Ca(OH)_2$ consumption, measuring 13 g/g SSA and 12 g/g SSA each. TGA results are consistent with the heat release analysis, where cumulative heat flow is higher with A1 and A2 than with A3 and A4. Ramanathan et al. [44] concluded that fly ash, pumice, glass, and metakaolin are pozzolanic and slag is hydraulic and highly reactive SCM classified according to the heat released in the function of $Ca(OH)_2$ consumption. Following their classification, the SSA of our study exhibits latent hydraulic and less reactive properties. We conclude that the studied ashes present an overall low reactivity, yet A1 and A2 are more reactive than A3 and A4, which is consistent with previous findings.

3.4.2. Reactivity Assessed Using Mechanical Properties

SAI is an indirect method to evaluate the pozzolanic activity of SCMs using compressive strength (Rc). Figure 6 displays the calculated SAI of the three ashes (A1, A2, and A3) at 1, 2, 7, and 28 days. In this experiment, A4 was not tested due to limited resources. At all ages, SAI is lower than 100%. This is attributed to a reduced compressive for all specimens with SSA replacing 25% OPC.

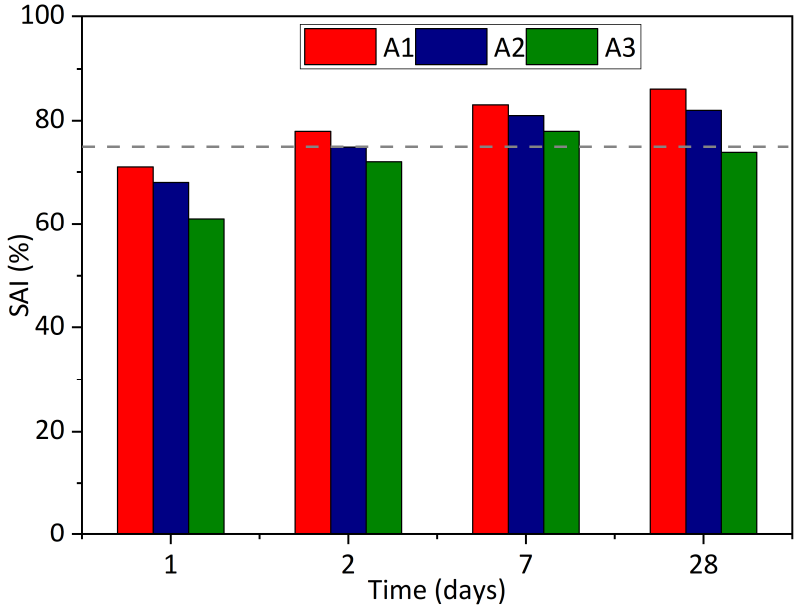

Figure 6. SAI of normalized mortar with 25 wt% SSA. The dotted grey line represents the requirement of 75% according to EN 450.

Mortars with A1 and A2 show a comparable trend of Rc increase over time, reaching 86% and 82%, respectively, at 28 days. Compared to that, mortar samples with A3 show an increase in SAI to 78% at 7 days then drops to 74% at 28 days. In fact, the measured compressive strength of mortar samples containing A3 remained constant between 7 and 28 days, unlike the reference specimen that increased. This has caused a decrease in SAI value at 28 days. All samples with an SSA present SAI values below 100%, confirming that the ashes have a low reactivity [5]. A 75% SAI belongs to 25% of OPC substitution by an inert material [45]. According to the Standard, the SAI value greater than 75% at 28 days proves that the ashes incorporated provide either a physical or chemical improvement in the cement matrix, which is the case for A1 and A2. Substituting 25 wt% of OPC by another material reduces the cement content in the mortar, resulting in less formation of C-S-H hydrate. Since C-S-H is responsible for improving the mechanical properties of cement composites, a lower C-S-H formation leads to a decrease in compressive strength. This leads to a lower SAI for SSA-blended mortars, as shown in Figure 6. Additionally, the porous nature of added SSA causes it to absorb a proportion of the mixing water for mortar preparation. As a result, the mortar holding SSA becomes firmer and less flowable. This leads to difficulties in the concrete casting on-site, developing a higher chance of pore creation within the specimen after hardening and, consequently, reducing the mechanical properties. This is commonly observed in previous studies [7,46,47]. Gupta et al. [48] also pointed out that the lack of reactive amorphous mineral phase is one of the reasons behind the negative impact of SCM on compressive strength. The slightly higher SAI for A1 and A2 may be linked to the slow pozzolanic activity. This results in the formation of additional C-S-H from A1 and A2 and improves the mechanical properties of the blended cement mortars. This finding aligns with previously discussed results.

As for A3, ettringite formation in aqueous solution was detected in 3.3.1. This behavior is expected to be similar after incorporation in cement composites, where additional ettrin-

gite formation may be observed. If that was the case, the additional ettringite formation was observed to negatively affect the mechanical properties of the mortars with A3. Linking electrical conductivity to reactivity tests proves that the ettringite formation in A3, detected using XRD at around 13 min after contact with water, and the high content in calcium oxide (≈48%), did not improve the mechanical properties of A3-blended cement mortars. However, further investigations should be considered regarding the ionic concentration in the bulk solution as it primarily affects the kinetics of the hydration reaction [49] and the mechanical properties.

The compressive strength results determined at 7 days were plotted in the function of the heat released at 7 days (Figure 5a) for A1, A2, and A3 individually, as shown in Figure 7. A strong correlation exists, with a calculated R^2 value of 0.93. This confirms the correlation between the heat released during the reactions of the R^3 test and the mechanical behavior of SCM-blended cement mortars, as previously explored by Li et al. [27].

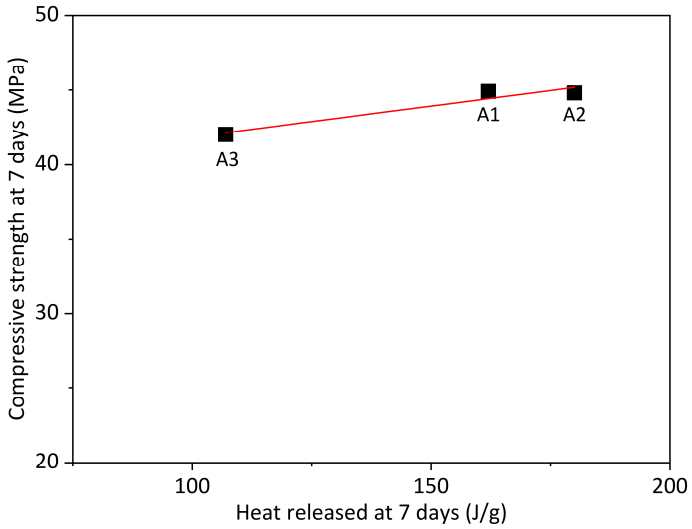

Figure 7. Correlation between the heat released after 7 days according to the R3 test results and the measured compressive strength at 7 days.

4. Conclusions

In this work, four SSAs were characterized, resulting from SS incineration with added limestone for toxic gas treatment. The addition of limestone to the incineration procedure influenced the chemical properties of SSA as it increased the Ca content in the ashes.

After studying the behavior of the four ashes in an aqueous solution for up to 8 days, the key findings are the following:

- A significant $Ca(OH)_2$ formation was observed after contact with water, due to the lime content in SSA, leading to a highly alkaline medium.
- A formation of ettringite only for A3 and A4 in aqueous solution.
- A decrease in electrical conductivity indicates slightly higher reactivity for A1 and A2.
- The heavy metal's leachability showed low concentrations, and the waste is therefore considered non-hazardous.
- In terms of reactivity assessment, the key findings are as follows:
- The four SSAs showed a low reactivity compared to other common SCMs such as slag and metakaolin.
- The SAI results of A1 and A2 presented a value higher than 75%, which confirms their reactivity.
- A strong correlation was confirmed between the heat release and the compressive strength of SSA blended cement mortars at 7 days.

Based on our findings, the application of SSA in cement composites showed promising mechanical properties, indicating that the tested ash can partially replace Portland cement

SCM. Further investigations are to be considered regarding the impact of SSA on cement mortar properties, as well as exploring activation mechanisms to improve SSA reactivity.

Author Contributions: Conceptualization, D.S., A.G. and P.G.; methodology, D.S. and A.G.; validation, A.G., P.G., H.K. and L.B.; formal analysis, D.S., A.G. and P.G.; investigation, D.S.; data curation, A.G.; writing—original draft preparation, D.S.; writing—review and editing, D.S., A.G., P.G., H.K., L.B., G.Z. and A.S.; visualization, A.G. and P.G.; supervision, A.G., P.G., H.K. and L.B. All authors have read and agreed to the published version of the manuscript.

Funding: This research received no external funding.

Data Availability Statement: The data may be made available upon request from the corresponding author (govin@emse.fr).

Acknowledgments: We express our sincere gratitude to VICAT and the FMI Process for providing the essential materials needed to accomplish the experimental part of this research.

Conflicts of Interest: Authors Hichem Krourm and Laetitia Bessette are employed by the company VICAT. Authors Gonzague Ziegler and Anthony Serclerat are employed by the company FMI Process. The remaining authors declare that the research was conducted in the absence of any commercial or financial relationships that could be construed as a potential conflict of interest.

References

1. Donatello, S.; Tyrer, M.; Cheeseman, C.R. EU Landfill Waste Acceptance Criteria and EU Hazardous Waste Directive Compliance Testing of Incinerated Sewage Sludge Ash. *Waste Manag.* **2010**, *30*, 63–71. [CrossRef] [PubMed]
2. Garcés, P.; Pérez Carrión, M.; García-Alcocel, E.; Payá, J.; Monzó, J.; Borrachero, M.V. Mechanical and Physical Properties of Cement Blended with Sewage Sludge Ash. *Waste Manag.* **2008**, *28*, 2495–2502. [CrossRef] [PubMed]
3. Donatello, S.; Cheeseman, C.R. Recycling and Recovery Routes for Incinerated Sewage Sludge Ash (ISSA): A Review. *Waste Manag.* **2013**, *33*, 2328–2340. [CrossRef]
4. Liu, D.-S.; Wang, C.-Q.; Mei, X.-D.; Huang, Q.; Ding, S.-M. An Effective Treatment Method for Shale Gas Drilling Cuttings Solidified Body. *Environ. Sci. Pollut. Res.* **2019**, *26*, 17853–17857. [CrossRef] [PubMed]
5. Haustein, E.; Kuryłowicz-Cudowska, A.; Łuczkiewicz, A.; Fudala-Książek, S.; Cieślik, B.M. Influence of Cement Replacement with Sewage Sludge Ash (SSA) on the Heat of Hydration of Cement Mortar. *Materials* **2022**, *15*, 1547. [CrossRef] [PubMed]
6. Smol, M.; Kulczycka, J.; Henclik, A.; Gorazda, K.; Wzorek, Z. The Possible Use of Sewage Sludge Ash (SSA) in the Construction Industry as a Way towards a Circular Economy. *J. Clean. Prod.* **2015**, *95*, 45–54. [CrossRef]
7. Maozhe, C.; Blanc, D.; Gautier, M.; Mehu, J.; Gourdon, R. Environmental and Technical Assessments of the Potential Utilization of Sewage Sludge Ashes (SSAs) as Secondary Raw Materials in Construction. *Waste Manag.* **2013**, *33*, 1268–1275.
8. Lynn, C.J.; Dhir, R.K.; Ghataora, G.S.; West, R.P. Sewage Sludge Ash Characteristics and Potential for Use in Concrete. *Constr Build. Mater.* **2015**, *98*, 767–779. [CrossRef]
9. Cyr, M.; Klysz, G.; Juilen, S.; Clastres, P. Les Cendres d'incinération de Boues de Station de Traitement Des Eaux Polluées Sont-Elles Utilisables Dans La Matrice Cimentaire? Comparaison avec les cendres volantes de charbon. *Environ. Ingénierie Développement* **2003**, *29*, 22–29.
10. Świerczek, L.; Cieślik, B.M.; Konieczka, P. Challenges and Opportunities Related to the Use of Sewage Sludge Ash in Cement-Based Building Materials—A Review. *J. Clean. Prod.* **2021**, *287*, 125054. [CrossRef]
11. Donatello, S.; Freeman-Pask, A.; Tyrer, M.; Cheeseman, C.R. Effect of Milling and Acid Washing on the Pozzolanic Activity of Incinerator Sewage Sludge Ash. *Cem. Concr. Compos.* **2010**, *32*, 54–61. [CrossRef]
12. Fontes, C.M.A.; Barbosa, M.C.; Toledofilho, R.D.; Gonçalves, J.P. Potentiality of Sewage Sludge as as Mineral Additive in Cement Mortar and High Performance Concrete. In Proceedings of the Conference: Use of Recycled Materials in Buildings and Structures, Barcelona, Spain, 8–11 November 2004; RILEM Publications: Champs-sur-Marne, France, 2004; pp. 797–806.
13. Pinheiro, V.D.; Alexandre, J.; Xavier, G.d.C.; Marvila, M.T.; Monteiro, S.N.; de Azevedo, A.R.G. Methods for Evaluating Pozzolanic Reactivity in Calcined Clays: A Review. *Materials* **2023**, *16*, 4778. [CrossRef] [PubMed]
14. Golewski, G.L. The Role of Pozzolanic Activity of Siliceous Fly Ash in the Formation of the Structure of Sustainable Cementitious Composites. *Sustain. Chem.* **2022**, *3*, 520–534. [CrossRef]
15. Cyr, M.; Coutand, M.; Clastres, P. Technological and Environmental Behavior of Sewage Sludge Ash (SSA) in Cement-Based Materials. *Cem. Concr. Res.* **2007**, *37*, 1278–1289. [CrossRef]
16. Van Caneghem, J.; Brems, A.; Lievens, P.; Block, C.; Billen, P.; Vermeulen, I.; Dewil, R.; Baeyens, J.; Vandecasteele, C. Fluidized Bed Waste Incinerators: Design, Operational and Environmental Issues. *Prog. Energy Combust. Sci.* **2012**, *38*, 551–582. [CrossRef]
17. Liu, J.; Zeng, J.; Sun, S.; Huang, S.; Kuo, J.; Chen, N. Combined Effects of $FeCl_3$ and CaO Conditioning on SO_2, HCl and Heavy Metals Emissions during the DDSS Incineration. *Chem. Eng. J.* **2016**, *299*, 449–458. [CrossRef]
18. Zacharczuk, W.; Andruszkiewicz, A.; Tatarek, A.; Alahmer, A.; Alsaqoor, S. Effect of Ca-Based Additives on the Capture of SO_2 during Combustion of Pulverized Lignite. *Energy* **2021**, *231*, 120988. [CrossRef]

19. Wolf, K.J.; Smeda, A.; Müller, M.; Hilpert, K. Investigations on the Influence of Additives for SO_2 Reduction during High Alkaline Biomass Combustion. *Energy Fuels* **2005**, *19*, 820–824. [CrossRef]
20. Qi, J.; Han, K.; Wang, Q.; Gao, J. Carbonization of Biomass: Effect of Additives on Alkali Metals Residue, SO_2 and NO Emission of Chars during Combustion. *Energy* **2017**, *130*, 560–569. [CrossRef]
21. Elled, A.L.; Åmand, L.E.; Leckner, B.; Andersson, B.Å. Influence of Phosphorus on Sulphur Capture during Co-Firing of Sewage Sludge with Wood or Bark in a Fluidised Bed. *Fuel* **2006**, *85*, 1671–1678. [CrossRef]
22. Xu, Y.; Zhang, L.; Chen, J.; Liu, T.; Li, N.; Xu, J.; Yin, W.; Li, D.; Zhang, Y.; Zhou, X. Phosphorus Recovery from Sewage Sludge Ash (SSA): An Integrated Technical, Environmental and Economic Assessment of Wet-Chemical and Thermochemical Methods. *J. Environ. Manag.* **2023**, *344*, 118691. [CrossRef] [PubMed]
23. Paya, J.; Borrachero, M.V.; Monzo, J.; Peris-Mora, E.; Amahjour, F. Enhanced Conductivity Measurement Techniques for Evaluation of Fly Ash Pozzolanic Activity. *Cem. Concr. Res.* **2000**, *31*, 41–49. [CrossRef]
24. de Azevedo Basto, P.; Savastano Junior, H.; de Melo Neto, A.A. Characterization and Pozzolanic Properties of Sewage Sludge Ashes (SSA) by Electrical Conductivity. *Cem. Concr. Compos.* **2019**, *104*, 103410. [CrossRef]
25. Delair, S.; Guyonnet, R.; Govin, A.; Guilhot, B. Study of Efflorescence Forming Process on Cementitious Materials. In Proceedings of the 5th International Conference on Concrete under Severe Conditions of Environment and Loading, Tours, France, 4–6 June 2007.
26. Gao, N.; Kamran, K.; Quan, C.; Williams, P.T. Thermochemical Conversion of Sewage Sludge: A Critical Review. *Prog. Energy Combust. Sci.* **2020**, *79*, 100843. [CrossRef]
27. Li, X.; Snellings, R.; Antoni, M.; Alderete, N.M.; Ben Haha, M.; Bishnoi, S.; Cizer, Ö.; Cyr, M.; De Weerdt, K.; Dhandapani, Y.; et al. Reactivity Tests for Supplementary Cementitious Materials: RILEM TC 267-TRM Phase 1. *Mater. Struct.* **2018**, *51*, 151. [CrossRef]
28. Zhang, J.; Scherer, G.W. Comparison of Methods for Arresting Hydration of Cement. *Cem. Concr. Res.* **2011**, *41*, 1024–1036. [CrossRef]
29. Juenger, M.C.G.; Snellings, R.; Bernal, S.A. Supplementary Cementitious Materials: New Sources, Characterization, and Performance Insights. *Cem. Concr. Res.* **2019**, *122*, 257–273. [CrossRef]
30. Coutand, M.; Cyr, M.; Clastres, P. Use of Sewage Sludge Ash as Mineral Admixture in Mortars. *Proc. Inst. Civ. Eng. Constr. Mater.* **2006**, *159*, 153–162. [CrossRef]
31. Xie, W.; Liu, K.; Pan, W.-P.; Riley, J.T. Interaction between Emissions of SO_2 and HCl in Fluidized Bed Combustors. *Fuel* **1999**, *78*, 1425–1436. [CrossRef]
32. Mejdi, M.; Saillio, M.; Chaussadent, T.; Divet, L.; Tagnit-Hamou, A. Hydration Mechanisms of Sewage Sludge Ashes Used as Cement Replacement. *Cem. Concr. Res.* **2020**, *135*, 106115. [CrossRef]
33. Assi, A.; Bilo, F.; Federici, S.; Zacco, A.; Depero, L.E.; Bontempi, E. Bottom Ash Derived from Municipal Solid Waste and Sewage Sludge Co-Incineration: First Results about Characterization and Reuse. *Waste Manag.* **2020**, *116*, 147–156. [CrossRef] [PubMed]
34. El Fami, N.; Ez-zaki, H.; Sassi, O.; Boukhari, A.; Diouri, A. Rheology, Calorimetry and Electrical Conductivity Related-Properties for Monitoring the Dissolution and Precipitation Process of Cement-Fly Ash Mixtures. *Powder Technol.* **2022**, *411*, 117937. [CrossRef]
35. Bullard, J.W.; Jennings, H.M.; Livingston, R.A.; Nonat, A.; Scherer, G.W.; Schweitzer, J.S.; Scrivener, K.L.; Thomas, J.J. Mechanisms of Cement Hydration. *Cem. Concr. Res.* **2011**, *41*, 1208–1223. [CrossRef]
36. Kang, S.M.; Na, S.H.; Lee, S.H.; Song, M.S.; Lee, W.G.; Song, Y.J. Effects of Ettringite Formation on the Compressive Strength of Mortar during Activation of Blast-Furnace Slag without Ordinary Portland Cement. *Mater. Res. Innov.* **2015**, *19*, 545–548. [CrossRef]
37. Blotevogel, S.; Ehrenberg, A.; Steger, L.; Doussang, L.; Kaknics, J.; Patapy, C.; Cyr, M. Ability of the R^3 Test to Evaluate Differences in Early Age Reactivity of 16 Industrial Ground Granulated Blast Furnace Slags (GGBS). *Cem. Concr. Res.* **2020**, *130*, 105998. [CrossRef]
38. Aubert, J.E.; Husson, B.; Sarramone, N. Utilization of Municipal Solid Waste Incineration (MSWI) Fly Ash in Blended Cement. Part 1: Processing and Characterization of MSWI Fly Ash. *J. Hazard. Mater.* **2006**, *136*, 624–631. [CrossRef]
39. Pacewska, B.; Wilińska, I. Usage of Supplementary Cementitious Materials: Advantages and Limitations: Part I. C–S–H, C–A–S–H and Other Products Formed in Different Binding Mixtures. *J. Therm. Anal. Calorim.* **2020**, *142*, 371–393. [CrossRef]
40. Decree of 12 December 2014. Available online: https://www.legifrance.gouv.fr (accessed on 2 April 2024).
41. Chang, Z.; Long, G.; Xie, Y.; Zhou, J.L. Chemical Effect of Sewage Sludge Ash on Early-Age Hydration of Cement Used as Supplementary Cementitious Material. *Constr. Build. Mater.* **2022**, *322*, 126116. [CrossRef]
42. Avet, F.; Li, X.; Ben Haha, M.; Bernal, S.A.; Bishnoi, S.; Cizer, Ö.; Cyr, M.; Dolenec, S.; Durdzinski, P.; Haufe, J.; et al. Report of RILEM TC 267-TRM Phase 2: Optimization and Testing of the Robustness of the R3 Reactivity Tests for Supplementary Cementitious Materials. *Mater. Struct.* **2022**, *55*, 92. [CrossRef]
43. Ali, H.A.; Xuan, D.; Poon, C.S. Assessment of Long-Term Reactivity of Initially Lowly-Reactive Solid Wastes as Supplementary Cementitious Materials (SCMs). *Constr. Build. Mater.* **2020**, *232*, 117192. [CrossRef]
44. Ramanathan, S.; Kasaniya, M.; Tuen, M.; Thomas, M.D.A.; Suraneni, P. Linking Reactivity Test Outputs to Properties of Cementitious Pastes Made with Supplementary Cementitious Materials. *Cem. Concr. Compos.* **2020**, *114*, 103742. [CrossRef]
45. Wang, Y.; Burris, L.; Shearer, C.R.; Hooton, D.; Suraneni, P. Strength Activity Index and Bulk Resistivity Index Modifications That Differentiate Inert and Reactive Materials. *Cem. Concr. Compos.* **2021**, *124*, 104240. [CrossRef]

46. Baeza-Brotons, F.; Garcés, P.; Payá, J.; Saval, J.M. Portland Cement Systems with Addition of Sewage Sludge Ash. Application in Concretes for the Manufacture of Blocks. *J. Clean. Prod.* **2014**, *82*, 112–124. [CrossRef]
47. Liang, C.; Le, X.; Fang, W.; Zhao, J.; Fang, L.; Hou, S. The Utilization of Recycled Sewage Sludge Ash as a Supplementary Cementitious Material in Mortar: A Review. *Sustainability* **2022**, *14*, 4432. [CrossRef]
48. Gupta, S.; Chaudhary, S. State of the Art Review on Supplementary Cementitious Materials in India—II: Characteristics of SCMs, Effect on Concrete and Environmental Impact. *J. Clean. Prod.* **2022**, *357*, 131945. [CrossRef]
49. Lavagna, L.; Nisticò, R. An Insight into the Chemistry of Cement—A Review. *Appl. Sci.* **2023**, *13*, 203. [CrossRef]